Journal of Power Sources 253 (2014) 294–299

Contents lists available at ScienceDirect

Journal of Power Sources

journal homepage: www.elsevier.com/locate/jpowsour

Short communication

Mesoporous $Li_3V_2(PO_4)_3$@CMK-3 nanocomposite cathode material for lithium ion batteries

Senlin Wang [a], Zhengxi Zhang [a,*], Zhitong Jiang [a], Aniruddha Deb [b], Li Yang [a,c,*], Shin-ichi Hirano [c]

[a] School of Chemistry and Chemical Engineering, Shanghai Jiao Tong University, Shanghai 200240, PR China
[b] Department of Chemistry, University of Michigan, Ann Arbor, MI 48109, USA
[c] Hirano Institute for Materials Innovation, Shanghai Jiao Tong University, Shanghai 200240, PR China

HIGHLIGHTS

- Mesoporous $Li_3V_2(PO_4)_3$@CMK-3 nanocomposite is synthesized via a sol–gel method.
- $Li_3V_2(PO_4)_3$ particles disperse both inside and outside CMK-3 mesoporous channels.
- The $Li_3V_2(PO_4)_3$@CMK-3 nanocomposite exhibits good electrochemical performance.

ARTICLE INFO

Article history:
Received 24 September 2013
Received in revised form
13 December 2013
Accepted 18 December 2013
Available online 27 December 2013

Keywords:
Lithium vanadium phosphate
Mesoporous carbon
Cathode material
Lithium ion batteries
Sol–gel method

ABSTRACT

The mesoporous $Li_3V_2(PO_4)_3$@CMK-3 nanocomposite has been firstly synthesized by a sol–gel method. The X-ray diffraction (XRD), transmission electron microscopy (TEM) and nitrogen adsorption–desorption measurements show that the $Li_3V_2(PO_4)_3$@CMK-3 nanocomposite exhibits the pure monoclinic structure and mesoporous morphology. $Li_3V_2(PO_4)_3$ has particle sizes of <50 nm, and are embedded in the mesoporous channels as well as well dispersed on the CMK-3 surface. Electrochemical measurements demonstrate that the $Li_3V_2(PO_4)_3$@CMK-3 nanocomposite shows significantly better rate capability and cycling performance than the bulk $Li_3V_2(PO_4)_3$. In the potential range of 3.0–4.3 V, the $Li_3V_2(PO_4)_3$@CMK-3 nanocomposite delivers high initial discharge capacity of 130.0 mAh g^{-1} at 0.2 C, and maintain an initial discharge capacity of 119.5 and 107.8 mAh g^{-1} at 5 C and 10 C, respectively. After 300 cycles, it can still retain a discharge capacity of 95.4 and 73.5 mAh g^{-1} at 5 C and 10 C, respectively. The good electrochemical performance for the $Li_3V_2(PO_4)_3$@CMK-3 nanocomposite are related to the special mesoporous structure, nanosized particles, and the existence of conductive carbon matrix, thus leading to improvement in electron and lithium ion diffusivity.

1. Introduction

Lithium ion batteries have attracted considerable attention as important energy storage and conversion systems for applications including electric vehicles (EVs), hybrid electric vehicles (HEVs) and smart grids, owing to their high energy and power density, as well as long cycle life. Recently, lithium transition metal phosphates, such as $LiFePO_4$, $LiMnPO_4$ and $Li_3V_2(PO_4)_3$, have been considered as potential cathode materials for lithium ion batteries, because the above-mentioned phosphates display much better electrochemical and thermal stability compared to conventional lithium metal oxide cathodes [1,2]. Among these phosphates, monoclinic $Li_3V_2(PO_4)_3$ is one of the most promising cathode materials due to its high theoretical capacity, high operating voltage, and safety performance [3,4].

Unfortunately, $Li_3V_2(PO_4)_3$ has an inherent low electronic conductivity (10^{-8}–10^{-7} S cm^{-1}) [3,5], which limits its practical application in the high-power batteries. Doping with alien ions [6–10] and coating with conductive materials such as metal [11], metal oxide [12], or carbon [13,14] are two main methods to enhance the electronic conductivity. Besides, fabricating nanosized particles is also an effective way. However, nanoscaled particles tends to aggregate during high temperature calcination and electrochemical process owing to the small size and high surface energy [15]. Thus,

* Corresponding authors. School of Chemistry and Chemical Engineering, Shanghai Jiao Tong University, Shanghai 200240, PR China. Tel: +86 21 54748917; fax: +86 21 54741297.
E-mail addresses: zhengxizhang@sjtu.edu.cn (Z. Zhang), liyangce@sjtu.edu.cn (L. Yang).

0378-7753/$ – see front matter © 2013 Elsevier B.V. All rights reserved.
http://dx.doi.org/10.1016/j.jpowsour.2013.12.080

how to maintain a uniform dispersion of $Li_3V_2(PO_4)_3$ nanoparticles is an important and challenging issue, especially in the area of high-power lithium ion batteries, because aggregation of nanoparticles result in the poor power performance. As reported previously, one of the most effective approach is embedding $Li_3V_2(PO_4)_3$ nanoparticles in the irregular porous carbon matrix, which can suppress the agglomeration of nanoparticles, thus improving the rate performance of nano-structured $Li_3V_2(PO_4)_3$ cathode materials [16–20].

In recent years, CMK-3, a kind of ordered mesoporous carbon frameworks, has been used as conductive and mesoporous matrix in lithium ion batteries, because it not only provides a fast ion/electron transport path and good contact of electrolyte with electrode material, but also acts as a rigid skeleton for active particles that prevents the aggregation and growth of nanoparticles. Some mesoporous electrode materials, including $LiFePO_4$ [21], Li_2MnSiO_4 [22], TiO_2 [23], $Li_4Ti_5O_{12}$ [24], MoS_2 [25], and SnO_2 [26], have been synthesized via using CMK-3 as a carbon matrix, which exhibit satisfactory electrochemical performance. For example, Wang et al. [21] developed highly ordered mesoporous $LiFePO_4$/C nanocomposite cathode materials by a two-step nanocasting technique, in which $LiFePO_4$ nanoparticles distributed both inside and outside mesopore channels in CMK-3 carbon matrix. The as-prepared $LiFePO_4$/C nanocomposite presented good rate capability and cycling performance at the low and high current rates, because of its mesoporous structure. In this work, we firstly report on a sol–gel method to synthesize the $Li_3V_2(PO_4)_3$@CMK-3 nanocomposite. The morphology and electrochemical performance of the as-prepared nanocomposite have been investigated. $Li_3V_2(PO_4)_3$ has particles size of less than 50 nm, and are anchored both inside and outside CMK-3 mesoporous channels. By comparison to the bulk $Li_3V_2(PO_4)_3$, the as-prepared $Li_3V_2(PO_4)_3$@CMK-3 nanocomposite exhibits improved electrochemical performance, especially at higher current rates, which can be attributed to its mesoporous structure, nanoscale $Li_3V_2(PO_4)_3$ particles and conductive carbon matrix.

2. Experimental

2.1. Synthesis of $Li_3V_2(PO_4)_3$@CMK-3 nanocomposite and bulk $Li_3V_2(PO_4)_3$

CMK-3 was purchased from Nanjing Xfnano Materials Tech Co., Ltd, China, and treated by nitric acid to enhance the hydrophilicity before use. The $Li_3V_2(PO_4)_3$@CMK-3 nanocomposite was synthesized by a sol–gel method. Firstly, 0.91 g vanadium pentoxide (V_2O_5) and 1.98 g oxalic acid dihydrate ($C_2H_2O_4 \cdot 2H_2O$) in a stoichiometric mole ratio of 1:3 were dissolved in deionized water under magnetic stirring at 50 °C. After a clear blue solution was obtained, a mixture of 1.73 g phosphoric acid (H_3PO_4, ≥85 wt% in H_2O) and 0.99 g lithium acetate (CH_3COOLi) was added to the above solution. While stirring for 1 h, then 0.2 g CMK-3 was added to the mixed solution and continues to stir at room temperature for another 12 h. The solution was stirred at 50 °C to evaporate the water and dried at 100 °C to remove the excess water. The precursor was pre-heated at 350 °C for 4 h under Ar atmosphere, then was grounded and calcined at 750 °C for 8 h under Ar atmosphere to yield $Li_3V_2(PO_4)_3$@CMK-3 nanocomposite.

The bulk $Li_3V_2(PO_4)_3$ was prepared by a sol–gel method as previous reported [27,28]. The synthesis route is the same to the $Li_3V_2(PO_4)_3$@CMK-3 except the citric acid was used to instead of CMK-3. The citric acid not only serves as a chelating agent but also as a carbon source.

2.2. Materials characterization

The structures of the as-prepared samples were characterized by X-ray diffraction measurement (XRD, Rigaku, D/max-RBusing Cu Kα radiation with $\lambda = 1.5418$ Å). The morphologies were examined by a transmission electron microscopy (JEM-2010HT). Surface areas were obtained by a N_2 adsorption analyzer (Micromeritics ASAP 2020). The carbon amounts were determined by C-S 00 infrared carbon–sulfur analyzer.

2.3. Electrochemical measurement

The galvanostatic charge–discharge tests of the as-prepared samples were conducted in CR2016 coin-type cells with a Land CT2001 battery tester at different C (1 C = 133 mAh g^{-1}) rates. The potential range was between 3.0 and 4.3 V, and the same charge and discharge rates were used. The mesoporous $Li_3V_2(PO_4)_3$@CMK-3 nanocomposite electrodes were prepared by using 80 wt% composite, 10 wt% carbon black, and 10 wt% polyvinylidene fluoride (PVDF). The bulk $Li_3V_2(PO_4)_3$ electrodes were prepared by using 75 wt% bulk $Li_3V_2(PO_4)_3$, 15 wt% carbon black, and 10 wt% PVDF. The weight of active material ($Li_3V_2(PO_4)_3$) was calculated by subtracting the weight of the residual carbon from total weight of the as-prepared samples. The active material loading was in the range of 1–2 mg cm^{-2}. The coin-type battery test cells (size 2016R), each of which contained a cathode, a Li metal anode, 1 M $LiPF_6$ in EC/DMC (1/1 vol %) as the electrolyte, and a glass fiber filter (Whatman, GF/A) as the separator, were fabricated in an argon-filled glove box (M. Braun Co., $[O_2] < 1$ ppm, $[H_2O] < 1$ ppm). Cyclic voltammetry dates were carried out with a CHI604b electrochemical workstation at a scan rate of 0.2 mV s^{-1} in the range of 3.0–4.3 V. Electrochemical impedance spectroscopy (EIS) measurement was obtained with a CHI604b electrochemical workstation in the frequency range of 100 kHz–10 mHz with an excitation voltage of 5 mV.

3. Results and discussion

Fig. 1 shows the XRD patterns of the $Li_3V_2(PO_4)_3$@CMK-3 composite and bulk $Li_3V_2(PO_4)_3$. It can be seen that both of two samples have the monoclinic single phase with the space group ($P2_1/n$), which are consistent with the previous report [3]. Moreover, no diffraction peaks of carbon are detected, suggesting that the carbon in the $Li_3V_2(PO_4)_3$@CMK-3 composite as well as in the bulk $Li_3V_2(PO_4)_3$ are amorphous, and do not affect the crystallize structure of $Li_3V_2(PO_4)_3$. The content of residual carbon is 10.1% for the $Li_3V_2(PO_4)_3$@CMK-3 composite, and 3.6% for the bulk $Li_3V_2(PO_4)_3$.

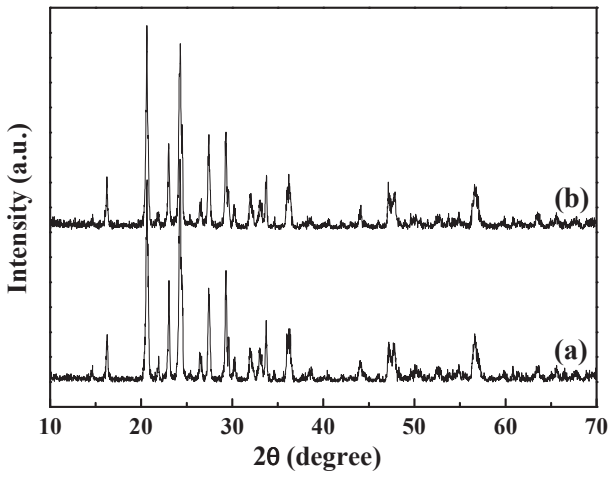

Fig. 1. XRD patterns of synthesized samples (a) $Li_3V_2(PO_4)_3$@CMK-3, (b) bulk $Li_3V_2(PO_4)_3$.

The morphology of as-obtained samples is analyzed by TEM. As shown in Fig. 2(a), CMK-3 has mesoporous channel structures with a uniform pore size of several nanometers. Fig. 2(b) and (c) presents TEM images of $Li_3V_2(PO_4)_3$@CMK-3 composite. It can be observed that the size of the $Li_3V_2(PO_4)_3$ particles is less than 50 nm, and $Li_3V_2(PO_4)_3$ nanoparticles are embedded in the mesoporous channels as well as distributed on the CMK-3 surface after impregnation and calcinations process. The $Li_3V_2(PO_4)_3$@CMK-3 composite has a nearly same mesoporous structure as that of CMK-3, which is beneficial to penetration of electrolyte into the mesopores and contact between electrolyte and $Li_3V_2(PO_4)_3$ active nanoparticles [21,25]. In addition, from the insert image in Fig. 2(c), the lattice spacing is clearly present, indicating single crystallinity of the as-prepared nanocomposite, which is in good agreement with the XRD result. The 0.37 nm space corresponds to the (121) crystal face of the nanocomposite [17]. Fig. 2(d) depicts a TEM image of the bulk $Li_3V_2(PO_4)_3$. Agglomerated particles with a large particle size of more than 100 nm and irregular structure can be found for the bulk $Li_3V_2(PO_4)_3$. Besides, the carbon layer coated on the surface of $Li_3V_2(PO_4)_3$ particles is not uniform.

The nitrogen adsorption–desorption measurements are employed to investigate the structure and the Brunauer–Emmett–Teller (BET) surface areas of the CMK-3, $Li_3V_2(PO_4)_3$@CMK-3 nanocomposite and bulk $Li_3V_2(PO_4)_3$, and the isotherms of above-mentioned samples are displayed in Fig. 3. Both CMK-3 and $Li_3V_2(PO_4)_3$@CMK-3 nanocomposite show a typical IV isotherms with a H_1 hysteresis loop at a relative pressure P/P_0 of around 0.5, which is characteristics of mesoporous materials [29]. On the other hand, the bulk $Li_3V_2(PO_4)_3$ shows a II isotherm, agreeing with typical adsorption for non-porous materials. The BET surface areas are 1075.2 $m^2\ g^{-1}$ and 92.9 $m^2\ g^{-1}$ for pure CMK-3 and $Li_3V_2(PO_4)_3$@CMK-3 nanocomposite, respectively.

The CV curves of the $Li_3V_2(PO_4)_3$@CMK-3 nanocomposite and bulk $Li_3V_2(PO_4)_3$ with a scanning rate of 0.2 mV s^{-1} in the range of 3.0–4.3 V are shown in Fig. 4. Both of them show three oxidation peaks and three corresponding reduction peaks, which are consistent well with lithium ion extraction/insertion during the phase transition processes: $Li_3V_2(PO_4)_3 \leftrightarrow Li_2V_2(PO_4)_3 \leftrightarrow LiV_2(PO_4)_3$ [30]. In the case of the $Li_3V_2(PO_4)_3$@CMK-3 nanocomposite, the oxidation peaks are located at 3.64, 3.72 and 4.14 V vs. Li/Li^+, and three corresponding reduction peaks are located at 4.00, 3.63 and 3.55 V vs. Li/Li^+. For the bulk $Li_3V_2(PO_4)_3$, the oxidation peaks are located at 3.68, 3.77 and 4.20 V vs. Li/Li^+, and three reduction peaks are located at 3.95, 3.58 and 3.48 V vs. Li/Li^+. Compared with the bulk $Li_3V_2(PO_4)_3$, the $Li_3V_2(PO_4)_3$@CMK-3 nanocomposite shows smaller potential difference between reduction peaks and oxidation peaks, suggesting that such nanocomposite has lower electrochemical polarization and better reversibility [17,31,32].

Fig. 5 shows the initial charge–discharge curves of the mesoporous $Li_3V_2(PO_4)_3$@CMK-3 and bulk $Li_3V_2(PO_4)_3$ electrodes in the potential range of 3.0–4.3 V at different rates. It is evident that both of them exhibit three charge plateaus and three discharge plateaus at the low rate of 0.2 C, corresponding to the two-phase transition process, which is similar to the CV result. When the rate is up to 5 C, the charge and discharge plateaus for the $Li_3V_2(PO_4)_3$@CMK-3 sample are still maintained, however, the plateaus for the bulk $Li_3V_2(PO_4)_3$ are not clearly visible. The mesoporous $Li_3V_2(PO_4)_3$@CMK-3 sample is able to deliver an initial discharge capacity of 130.0 mAh g^{-1} at the rate of 0.2 C, which is close to the theoretical capacity (133 mAh g^{-1}). Although increasing current rate leads to a decrease in the discharge capacity, high initial discharge capacities of 127.2, 125.5, 124.0, 119.5 and 107.8 mAh g^{-1} can still be reached at the rate of 0.5 C, 1 C, 2 C, 5 C and 10 C, respectively, indicating that the nanocomposite has good rate capability. In comparison, the bulk $Li_3V_2(PO_4)_3$ sample delivers initial discharge capacities of 122.1, 119.5, 116.7, 112.9 and 100.3 mAh g^{-1} at the rate of 0.2 C, 0.5 C, 1 C, 2 C and 5 C, respectively. Clearly, the $Li_3V_2(PO_4)_3$@CMK-3 nanocomposite exhibits higher initial discharge capacities than the bulk $Li_3V_2(PO_4)_3$, and this difference enhances at higher current rates.

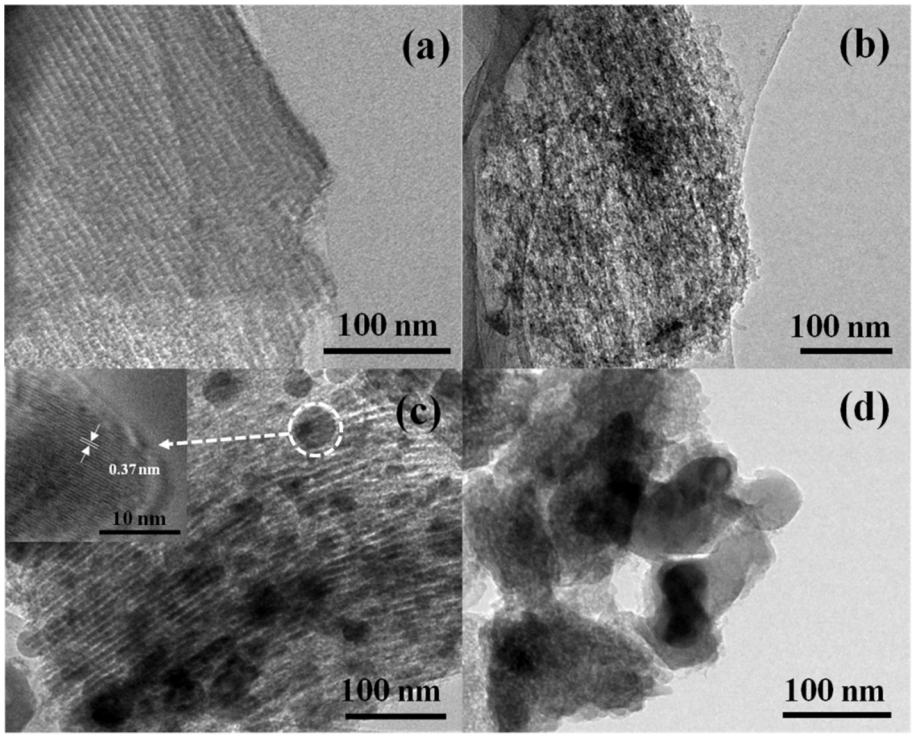

Fig. 2. TEM images of the (a) CMK-3, (b, c) $Li_3V_2(PO_4)_3$@CMK-3, (d) bulk $Li_3V_2(PO_4)_3$.

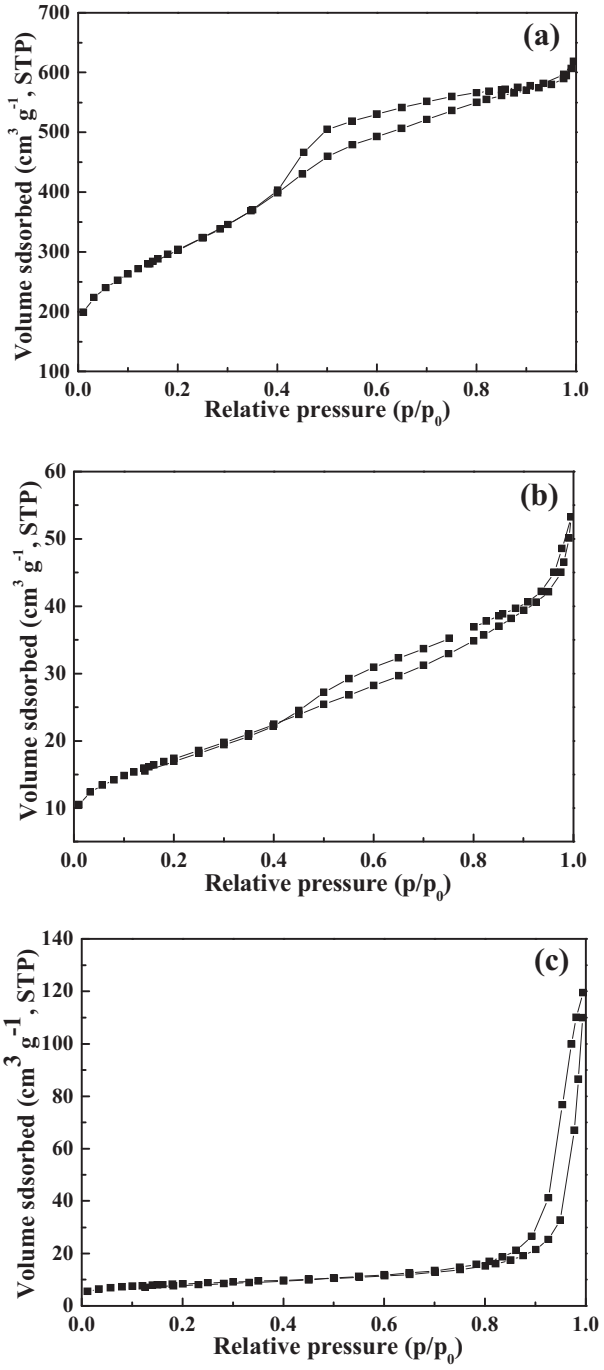

Fig. 3. Nitrogen adsorption–desorption isotherms of the (a) CMK-3, (b) $Li_3V_2(PO_4)_3$@CMK-3, (c) bulk $Li_3V_2(PO_4)_3$.

In order to investigate the cycle life of as-prepared samples, the cycling performance at different rates was examined and displayed in Fig. 6. It is observed that the $Li_3V_2(PO_4)_3$@CMK-3 sample shows acceptable cycling performance. After 100 cycles, it can present discharge capacities of 126.3 mAh g^{-1} with 97.2% capacity retention and 123.8 mAh g^{-1} with 97.3% capacity retention at 0.2 C and 0.5 C, respectively. When operated at 1 C, 2 C, 5 C and 10 C, the discharge capacities of 119.5, 110.4, 95.4 and 73.5 mAh g^{-1} can be obtained after 300 cycles, respectively. On the other hand, the bulk $Li_3V_2(PO_4)_3$ sample delivers discharge capacity of 111.4 mAh g^{-1} with 95.5% capacity retention after 100 cycles at 1 C. Recently,

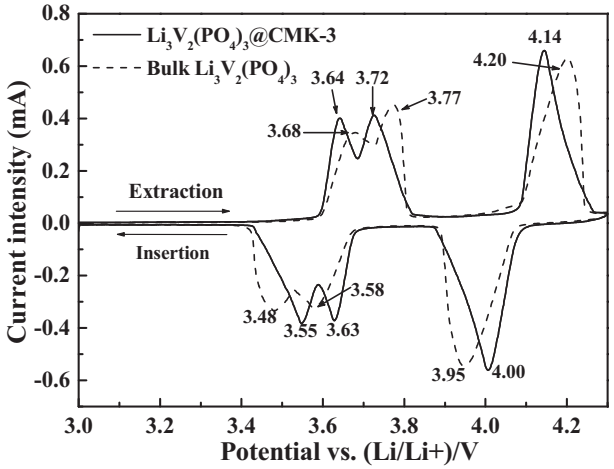

Fig. 4. CV curves of the as-prepared $Li_3V_2(PO_4)_3$@CMK-3 nanocomposite and bulk $Li_3V_2(PO_4)_3$ at a scan rate of 0.2 mV s^{-1} in the range of 3.0–4.3 V.

Böckenfeld et al. [28] synthesized two different $Li_3V_2(PO_4)_3$ samples via a sol–gel method, and found that $Li_3V_2(PO_4)_3$ electrodes can be successfully used as cathode and anode materials in different half-cell configurations and electrochemical devices.

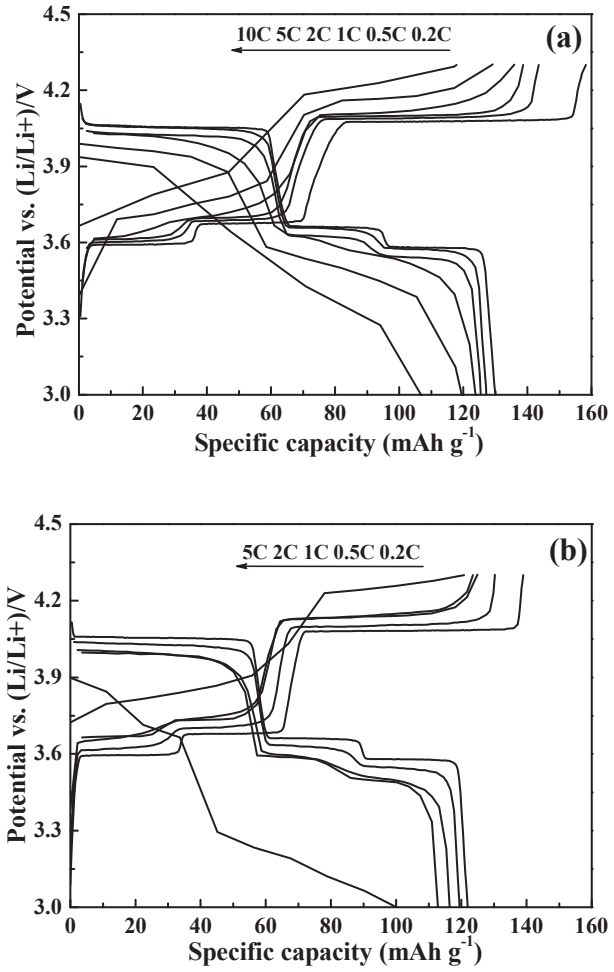

Fig. 5. Initial charge–discharge curves of (a) $Li_3V_2(PO_4)_3$@CMK-3 and (b) bulk $Li_3V_2(PO_4)_3$ electrode in the range of 3.0–4.3 V at various rates.

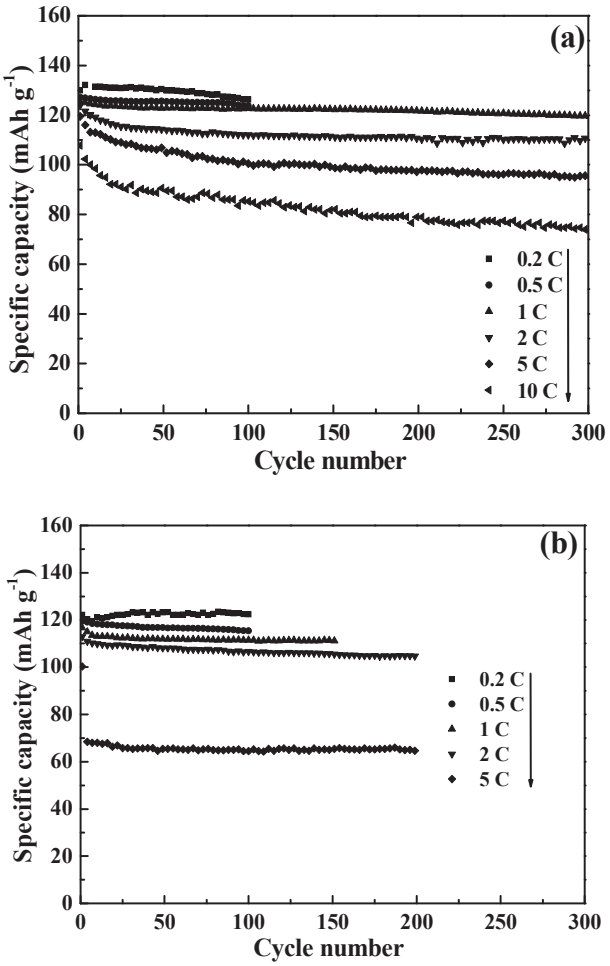

Fig. 6. Cycle performances of (a) $Li_3V_2(PO_4)_3$@CMK-3 and (b) bulk $Li_3V_2(PO_4)_3$ electrode in the range of 3.0–4.3 V at various rates.

When $Li_3V_2(PO_4)_3$ electrodes are used as cathode materials in half-cell configurations, the capacity retention of the bulk $Li_3V_2(PO_4)_3$ sample prepared in our work is similar to that of the $Li_3V_2(PO_4)_3$ sample synthesized by Böckenfeld et al. at 1 C. Additionally, it can be seen that when the current rate is increased to 5 C, the discharge capacity of the bulk $Li_3V_2(PO_4)_3$ sample prepared in our work decreases rapidly at the initial cycles, and then only retain about 65.0 mAh g^{-1} after several cycles.

As expected, the $Li_3V_2(PO_4)_3$@CMK-3 sample exhibits better rate capability and cycling performance than the bulk $Li_3V_2(PO_4)_3$, arising from the following several factors. Firstly, the $Li_3V_2(PO_4)_3$@CMK-3 sample has a mesoporous structure, which allow the electrolyte to penetrate into the mesopores easily and provide good contact between the electrolyte and $Li_3V_2(PO_4)_3$ nanoparticles. Secondly, nanosized $Li_3V_2(PO_4)_3$ particles (<50 nm) decrease the diffusion distance of lithium ions, which is favorable for lithium ion extraction and insertion [16,20]. Finally, the carbon framework can improve electronic conductivity of the nanocomposite and accelerate electron transport [21–26].

To further understand the electrochemical kinetic properties of as-prepared samples, electrochemical impedance spectroscopy (EIS) measurements are carried out, and the corresponding Nyquist plots are shown in Fig. 7(a). Both samples have similar EIS curves. The small intercept is related to the solution resistance (R_s); the depressed semicircle in the middle frequency represents the charge-transfer resistance (R_{ct}) and the double-layer capacitance (C_{dl}); the sloping line in the low frequency is attributed to Warburg impedance associated with the diffusion of lithium ions in the electrode (Z_w) [33]. An equivalent circuit model w displayed in the insert of Fig. 7(a) for analyzing impedance spectra. The R_{ct} value of the $Li_3V_2(PO_4)_3$@CMK-3 sample is much smaller (108.3 Ω) than that of the bulk $Li_3V_2(PO_4)_3$ (311.7 Ω), demonstrating that the electrons can transfer more easily between $Li_3V_2(PO_4)_3$ particles and the electrolyte for the $Li_3V_2(PO_4)_3$@CMK-3 sample, as a result of its mesoporous structure [34] and better carbon network [24]. Fig. 7(b) presents the linear fittings of Z' vs. square root of frequency ($\omega^{-1/2}$) in the low frequency region. In comparison with the bulk $Li_3V_2(PO_4)_3$, the $Li_3V_2(PO_4)_3$@CMK-3 sample has a lower slope, indicating higher lithium ion diffusion coefficient of such sample, which is derived from the nanoscale $Li_3V_2(PO_4)_3$ particles [35].

4. Conclusions

In summary, we have successfully fabricated the mesoporous $Li_3V_2(PO_4)_3$@CMK-3 nanocomposite by a sol–gel method. The size of the $Li_3V_2(PO_4)_3$ particles is less than 50 nm, and $Li_3V_2(PO_4)_3$ nanoparticles disperse uniformly both inside and outside CMK-3 mesoporous channels. Compared to the bulk $Li_3V_2(PO_4)_3$, the as-prepared $Li_3V_2(PO_4)_3$@CMK-3 nanocomposite exhibits much improved electrochemical performance, particularly at higher current rates. The results should be attributed to the mesoporous structure, nanosized particles as well as conductive carbon framework for $Li_3V_2(PO_4)_3$@CMK-3 nanocomposite, which can enhance the electronic conductivity and lithium ion diffusion.

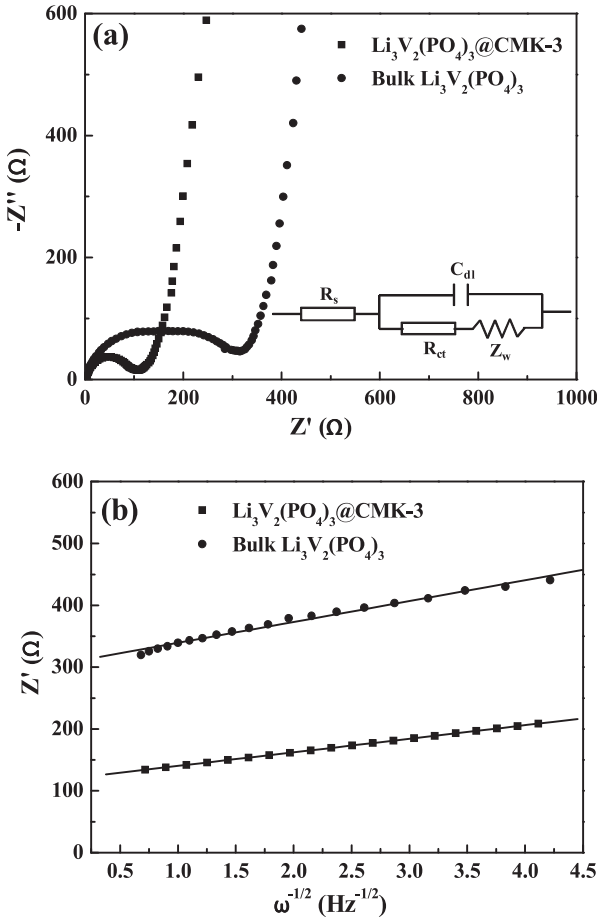

Fig. 7. (a) Nyquist plots of as-prepared samples, (b) the relationship between Z' and $\omega^{-1/2}$ in the low frequency region.

Acknowledgments

The authors are indebted to the University of Michigan–Shanghai Jiao Tong University 2012 Collaborative Research Project.

References

[1] S.K. Martha, J. Grinblat, O. Haik, E. Zinigrad, T. Drezen, J.H. Miners, I. Exnar, A. Kay, B. Markovsky, D. Aurbach, Angew. Chem. Int. Ed. 48 (2009) 8559–8563.
[2] M.S. Whittingham, Y. Song, S. Lutta, P.Y. Zavalij, N.A. Chernova, J. Mater. Chem. 15 (2005) 3362–3379.
[3] S.C. Yin, H. Grondey, P. Strobel, M. Anne, L.F. Nazar, J. Am. Chem. Soc. 125 (2003) 10402–10411.
[4] S.C. Yin, H. Grondey, P. Strobel, H. Huang, L.F. Nazar, J. Am. Chem. Soc. 125 (2003) 326–327.
[5] S.C. Yin, P.S. Strobel, H. Grondey, L.F. Nazar, Chem. Mater. 16 (2004) 1456–1465.
[6] J.S. Huang, L. Yang, K.Y. Liu, Y.F. Tang, J. Power Sources 195 (2010) 5013–5018.
[7] G. Bai, Y. Yang, H. Shao, J. Electroanal. Chem. 688 (2013) 98–102.
[8] H. Liu, S. Bi, G. Wen, X. Teng, P. Gao, Z. Ni, Y. Zhu, F. Zhang, J. Alloys Compd. 543 (2012) 99–104.
[9] R. Wang, S. Xiao, X. Li, J. Wang, H. Guo, J. Alloys Compd. 575 (2013) 268–272.
[10] S. Zhang, Q. Wu, C. Deng, F.L. Liu, M. Zhang, F.L. Meng, H. Gao, J. Power Sources 218 (2012) 56–64.
[11] L. Zhang, X.L. Wang, J.Y. Xiang, Y. Zhou, S.J. Shi, J.P. Tu, J. Power Sources 195 (2010) 5057–5061.
[12] J. Zhai, M. Zhao, D. Wang, Y. Qiao, J. Alloys Compd. 502 (2010) 401–406.
[13] M.M. Ren, Z. Zhou, X.P. Gao, W.X. Peng, J.P. Wei, J. Phys. Chem. C 112 (2008) 5689–5693.
[14] L. Wang, X. Jiang, X. Li, X. Pi, Y. Ren, F. Wu, Electrochim. Acta 55 (2010) 5057–5062.
[15] Y.-G. Guo, J.-S. Hu, L.-J. Wan, Adv. Mater. 20 (2008) 2878–2887.
[16] A. Pan, J. Liu, J.G. Zhang, W. Xu, G. Cao, Z. Nie, B.W. Arey, S. Liang, Electrochem. Commun. 12 (2010) 1674–1677.
[17] B. Pei, Z. Jiang, W. Zhang, Z. Yang, A. Manthiram, J. Power Sources 239 (2013) 475–482.
[18] X. Rui, D. Sim, K. Wong, J. Zhu, W. Liu, C. Xu, H. Tan, N. Xiao, H.H. Hng, T.M. Lim, Q. Yan, J. Power Sources 214 (2012) 171–177.
[19] L. Mai, S. Li, Y. Dong, Y. Zhao, Y. Luo, H. Xu, Nanoscale 5 (2013) 4864–4869.
[20] W. Duan, Z. Hu, K. Zhang, F. Cheng, Z. Tao, J. Chen, Nanoscale 5 (2013) 6485–6490.
[21] G. Wang, H. Liu, J. Liu, S. Qiao, G.M. Lu, P. Munroe, H. Ahn, Adv. Mater. 22 (2010) 4944–4948.
[22] T. Kawase, H. Yoshitake, Microporous Mesoporous Mater. 155 (2012) 99–105.
[23] L. Shen, E. Uchaker, C. Yuan, P. Nie, M. Zhang, X. Zhang, G. Cao, ACS Appl. Mater. Interfaces 4 (2012) 2985–2992.
[24] L. Shen, X. Zhang, E. Uchaker, C. Yuan, G. Cao, Adv. Energy Mater. 2 (2012) 691–698.
[25] X. Zhou, L.-J. Wan, Y.-G. Guo, Nanoscale 4 (2012) 5868–5871.
[26] H. Qiao, J. Li, J. Fu, D. Kumar, Q. Wei, Y. Cai, F. Huang, ACS Appl. Mater. Interfaces 3 (2011) 3704–3708.
[27] Y. Li, Z. Zhou, X. Gao, J. Yan, Electrochim. Acta 52 (2007) 4922–4926.
[28] N. Böckenfeld, A. Balducci, J. Power Sources 235 (2013) 265–273.
[29] R. Ryoo, S.H. Joo, M. Kruk, M. Jaroniec, Adv. Mater. 13 (2001) 677–681.
[30] Y.Q. Qiao, X.L. Wang, J.Y. Xiang, D. Zhang, W.L. Liu, J.P. Tu, Electrochim. Acta 56 (2011) 2269–2275.
[31] Y.Q. Qiao, J.P. Tu, X.L. Wang, D. Zhang, J.Y. Xiang, Y.J. Mai, C.D. Gu, J. Power Sources 196 (2011) 7715–7720.
[32] D. Ai, K. Liu, Z. Lu, M. Zou, D. Zeng, J. Ma, Electrochim. Acta 56 (2011) 2823–2827.
[33] M.V. Reddy, G.V. Subba Rao, B.V.R. Chowdari, J. Phys. Chem. C 111 (2007) 11712–11720.
[34] X. Zhang, S. Liu, K. Huang, S. Zhuang, J. Guo, T. Wu, P. Cheng, J. Solid State Electrochem. 16 (2011) 937–944.
[35] W. Yuan, J. Yan, Z. Tang, O. Sha, J. Wang, W. Mao, L. Ma, Electrochim. Acta 72 (2012) 138–142.